Electric Dichroism and Birefringence Decay of Short DNA Restriction Fragments Studied by Brownian Dynamics Simulation

S. A. Allison* and P. Nambi

Department of Chemistry, Georgia State University, Atlanta, Georgia 30303

Received June 10, 1991; Revised Manuscript Received October 15, 1991

ABSTRACT: Brownian dynamics simulation is used to study the electric dichroism (ED) and birefringence (EB) off-field decay of short DNA fragments 100–367 base pairs in length. The simulation results are compared to the ED experiments of Diekmann and co-workers (Diekmann, S.; et al. *Biophys. Chem.* **1982**, *15*, 263) and EB experiments of Lewis and co-workers (Lewis, R. J.; et al. *Macromolecules* **1986**, *19*, 134). It is found that a simple flexible wormlike chain model with a persistence length slightly larger than 50 nm is entirely consistent with the ED/EB decay of all fragments. Although rigid ensemble models are able to account reasonably well for the longest relaxation time, the faster decay process, which is particularly sensitive to chain flexibility, cannot be reproduced by such models. Averages appropriate for ED/EB decay are derived in an appendix (strictly valid at low field strengths) for an induced dipole and a saturation-induced dipole orienting mechanism, respectively. These averages are based on a simple form for the electric polarizability tensor which scales, in the case of a rodlike polyion, as the square of the molecular weight. ED/EB decays are compared for both cases and shown to be similar.

I. Introduction

Over the last 20 years, there has been a great deal of interest in the flexibility of DNA because of its importance in controlling expression, replication, and packing.[1-3] This flexibility is undoubtedly correlated with equilibrium conformation. If, for example, DNA is modeled as a uniform elastic tube with the unbent (straight-rod) conformation corresponding to the lowest energy state, thermal activation forces the molecule to adopt a wormlike chain conformation.[4,5] Under these conditions, the persistence length, P, can be related to the bending rigidity, κ, by the relation $\kappa = k_BTP$ where k_B is Boltzmann's constant and T is the absolute temperature. P for DNA has been determined from equilibrium conformation by a number of different techniques, and these results are reviewed elsewhere.[6] Despite differences there is now a consensus that P lies around 50 nm for native DNA under physiological salt conditions. Below an ionic strength of $I = 0.01$ M somewhat higher P's have been reported which is presumably due to electrostatic repulsions along the DNA backbone. (At $I = 0.002$ M, $P \approx 58$–75 nm.[7]) Electric birefringence (EB)[8-11] and dichroism (ED)[12-15] are two physical methods that have been used to estimate P. The longest lifetime component of EB/ED off-field decay has been attributed to the end-over-end rotational diffusion constant, $D_\perp$, of the DNA fragment. It is possible to determine $D_\perp$ for rigid ensembles of wormlike chains.[16] Assuming internal motion does not contribute to $D_\perp$ (or, more precisely, the longest lifetime component, $\tau_0 = (6D_\perp)^{-1}$, from EB or ED off-field decays), it is possible to to infer P from these measurements for monodisperse fragments of known contour length.[10]

The measurements discussed in the previous paragraph are based on equilibrium conformation or at least are interpreted in terms of models which depend only on static conformation. Dynamical interpretations such as the direct determination of κ have been impeded due to the complexity of stiff-chain dynamical models.[17-28] These models may work well under certain limiting conditions for certain types of experiments but not for others. For example, general Gaussian models[19] work well for chains with little stiffness while the normal-mode theory of Schurr and co-workers is limited to stiff chains and short times.[28] Perhaps the most promising general analytic theory of wormlike chains is that of Aragon and co-workers[26,27] which is still in the developmental stages. Nonetheless, interpretation of experiments like EB and ED decay in terms of dynamical models is important for several reasons. First, it has not been firmly established whether or not rigid models accurately predict $D_\perp$ for flexible wormlike chains. Preliminary studies indicate such models underestimate $D_\perp$.[29] Second, there is no a priori reason to expect the *apparent* bending rigidity, $\kappa_{app} = k_BTP$, to equal the actual bending rigidity since this is strictly valid only for a simple elastic model for bending. It has been well established that statically bent regions of DNA are associated with specific base pair sequences,[30-34] and in these cases at least the simple elastic model is inappropriate. In an extreme case, it is conceivable that a macromolecule could be highly curved due to static bends but at the same time have a very high bending rigidity. In fact recent analyses of transient photodichroism,[35] electric dichroism,[36] and electron spin resonance (Bruce Robinson, University of Washington, personal correspondence) of DNA indicate that κ may be from 2 to 4 times larger than κ_{app}.

In this work fairly realistic dynamical modeling studies of ED and EB decay experiments on monodisperse DNA fragments in the size range of 100–367 base pairs (bp) are carried out. In doing so, we shall correlate τ_0 with P and assess previous analyses involving rigid ensembles. In addition, the simple elastic bending model shall be studied thoroughly in order to determine how well it accounts for the actual decays observed experimentally. These studies are carried out using the technique of Brownian dynamics simulation, which has proven very useful in the study of polymer motion in solution.[37-42] Briefly, a time correlation function is obtained by carrying out a large number of dynamical trajectories of individual chains and calculating the necessary averages corresponding to the experimental observable. The chain model used is general enough to account for hydrodynamic interaction, bending and stretching flexibility, and finite chain length. In order to determine how sensitive ED/EB decay is to dynamical flexibility, parallel simulations of flexible and rigid chains (frozen in their starting configurations) are carried out. The resultant EB/ED decays are analyzed with CONTIN, which estimates the distribution of relaxation times that comprise the correlation function.[43] This sophisticated and readily available program is rapidly becoming a "standard" data analysis method which requires only

0024-9297/92/2225-0759$03.00/0

modest assumptions about the correlation functions being analyzed such as the range of possible lifetimes present and that the amplitude components of these lifetimes are positive.[11,29,44] CONTIN analysis of ED/EB decays usually yields two relaxation processes with lifetimes τ_0 and τ_1, and their associated amplitudes a_0 and a_1, where the 0 subscript refers to the longest lifetime component. We shall be particularly interested in the faster decay time τ_1, which will be referred to as the first internal time in this work.

The mechanism by which polyions are oriented in an applied external field is a complicating feature in the interpretation of both EB and ED measurements. Field reversal experiments have shown that DNA is oriented entirely by induced moments.[45] Furthermore, Kerr law behavior is exhibited by shorter fragments (less than 400 bp) at low fields (E less than about 5 kV/cm) which is also consistent with an induced dipole mechanism.[8,9,15] In this work, however, we are particularly interested in electric dichroism experiments carried out by Diekmann and coworkers at high electric fields.[12,13] At high fields, the steady-state dichroism varies linearly with $1/E$, which indicates the induced dipole saturates.[8,46,47] An empirical model which has been used with some success is the saturation-induced dipole (SID) model[15,48-50] which assumes the induced moment of the polyion saturates to a field-independent value above some critical field strength. The SID model is qualitatively consistent with the observed high field strength dependence of steady-state birefringence and dichroism.[51] However, Rau and Charney[52] and Charney[53] have pointed out inconsistencies in this model with regards to both high-field experiments and their own microscopic theory.[52] In particular, this theory, which models the polyion as an immobile charged rod surrounded by a Debye–Hückel ion atmosphere, predicts that the dipole moment attains a maximum value and then actually decreases as the field is increased further. Although the Rau and Charney theory is approximate in a number of important respects such as modeling the polyion as a rod, treating the ion atmosphere at the level of the Debye–Hückel approximation, and neglecting polyion transport, it represents the most realistic microscopic treatment of rodlike polyion polarization in external fields that is currently available.

The orientation mechanism is important in the present work since it influences the correlation function that needs to be computed in making a comparison between theory and experiment. On the other hand, it is clear from the previous paragraph that the orienting mechanism is complex and not well understood at the present time. An additional problem concerns the functional form of the electric polarizability tensor, χ, for a charged linear macromolecule. In previous work, it was simply assumed that χ could be modeled as the tensor sum over the individual virtual bond polarizabilities.[29] If this were true, however, the molecular polarizability tensor should vary linearly with molecular weight, M, for nearly rodlike polyions. For DNA, a nearly M^2 dependence is observed for fragments in the size range 150–2500 base pairs.[8,9,53] In Appendix A, a simple model[54] is considered which leads to a double-sum formula for χ (eq A7) which has the correct length dependence. In Appendix B, this result is used to derive an expression (eq B24) for the low-field transient electric birefringence decay for an induced dipole (ID) orienting mechanism. A somewhat different expression is obtained if an SID model is assumed (eq B16). In the case of the high-field dichroism experiments,[13] eq B16 is more appropriate because of dipole saturation. (Incidentally, eq B16 has the same functional form as the correlation function used in previous studies based on a purely induced electric dipole model.[29] However, in the present work account is taken of the more realistic form of χ as well as dipole saturation.)

In this work, interpretational problems which arise as a consequence of the complex nature of polyion alignment in electric fields are approached by analyzing the Brownian dynamics trajectories for both SID (eq B16) and ID (eq B24) orienting mechanisms. Although our starting models are crude, a comparison of the two will show how sensitive transient electrooptical behavior is to dipole saturation. Furthermore, the ED measurements on short DNA fragments of Diekmann and co-workers[13] show that the first internal time, τ_1 (but not a_1), is essentially independent of field strength. This suggests that ED/EB lifetimes, which are of primary interest in this work, are insensitive to field strength. Consequently, it is reasonable to compare lifetimes obtained from experiments at high electric fields to values obtained from model studies that are strictly valid only at low fields.

II. Methods

Basic Chain Model. Unless the polymer length or the simulation time of interest is extremely short, it is necessary to resort to models that contain less detail than "atomic" models currently used in molecular dynamics. This is certainly true in this work, where DNA fragments in the 100–370 base pair size range are modeled and trajectory times out to a maximum of about 100 μs are needed. Furthermore, in order to obtain birefringence or dichroism decay curves with high signal to noise ratios, several hundred independent trajectories per simulation must be carried out and the results averaged. In this work, a "trajectory" refers to the dynamical evolution of a single chain initially selected at random from an equilibrium ensemble.

A model used to represent a linear macromolecule in Brownian dynamics simulation has been described in detail previously.[55] Briefly, the polymer is modeled as a string of N identical beads of radius a held together by bending (U^b) and stretching (U^s) potentials

$$\beta U^b = \frac{g}{2}\sum_{j=1}^{N-2}\theta_j^2 \tag{1}$$

$$\beta U^s = \frac{c}{2}\sum_{j=1}^{N-1}\left(\frac{b_j - b_0}{b_0}\right)^2 \tag{2}$$

where $\beta = 1/k_BT$, g and c are dimensionless force constants for bending and stretching, respectively, θ_j is the angle between virtual bonds j and $j+1$, b_j is the length of bond j, and b_0 corresponds to the minimum in the stretching potential of an individual virtual bond. Overall, five parameters need to be specified: N, c, a, b_0, and g. A more general model which also includes torsion and (optionally) anisotropic bending has been described previously.[35] The effect of torsion is briefly discussed in the Conclusion.

In order to parametrize the chain following the procedure discussed below, it is important to have a means of estimating overall transport properties. In the equilibrium ensemble simulation (EES) method, a chain is selected from an equilibrium distribution and treated as a rigid structure.[16] The algorithm of Garcia de la Torre and coworkers[54] is then used to calculate the rotational diffusion tensor, $\mathbf{D}_r$, of the structure. (The algorithm can also be used to calculate the translational diffusion tensor and the center of diffusion. In the present application,

however, these are unnecessary.) It is then straightforward to diagonalize $\mathbf{D}_r$, and obtain rotational eigenvalues λ_{ri} where $\lambda_{r1} \leq \lambda_{r2} \leq \lambda_{r3}$. This procedure is repeated on an ensemble of chains (typically several hundred) in order to obtain averaged eigenvalues $\langle\lambda_{ri}\rangle$.

Selection of Chain Parameters. In this work, we are primarily interested in the contribution of internal motion to electric birefringence (EB) and dichroism (ED) decay. As shown in the first subsection of the Results portion of this paper as well as in previous work,[29] the EB or ED decays of different rigid chains are very similar if the $\langle\lambda_{ri}\rangle$'s match. In other words, a relatively crude 10 subunit chain, for example, can be found which mimics the EB decay of a more realistic 40 subunit Hagermann–Zimm (HZ) chain if they behave as rigid bodies and their rotational eigenvalues match. A Hagermann–Zimm chain consists of a string of touching beads with parameters N and a chosen to yield transport properties appropriate for a wormlike chain of contour length L, persistence length P, and diameter d.[16] Hence, our chains will be parametrized such that they match the $\langle\lambda_{ri}\rangle$'s of the appropriate HZ or wormlike chain.

The parameters N and c are chosen and the remaining three determined by iteration. In most cases, we set N = 10 (for reasons of computational efficiency) and c = 100. This choice of c yields a root-mean-square (rms) fluctuation in virtual bond length of about $b_0/10$ with $\langle b\rangle = 1.0194b_0$ and $\langle b^2\rangle^{1/2} = 1.0246b_0$.[55] As a first estimate, we choose b_0 (call it b_0') so that $\langle b\rangle = L/(N-1)$. For a wormlike chain, the mean-square end-to-end distance is

$$\langle R^2\rangle = 2LP\left[1 - \frac{P}{L}\left(1 - \exp\left(-\frac{L}{P}\right)\right)\right] \tag{3}$$

For our model chain, we find that g' which gives the correct $\langle R^2\rangle$ using the equation[55]

$$\langle R^2\rangle = (N-1)\langle b^2\rangle + \frac{2\alpha\langle b\rangle^2}{(1-\alpha)}\left((N-2) - \frac{\alpha - \alpha^{N-1}}{1-\alpha}\right) \tag{4}$$

where

$$\alpha = \langle\cos\theta\rangle = \frac{\int_0^\pi \cos\theta \sin\theta \exp\left(-\frac{g\theta^2}{2}\right) d\theta}{\int_0^\pi \sin\theta \exp\left(-\frac{g\theta^2}{2}\right) d\theta} \tag{5}$$

It is straightforward to integrate eq 5 and construct a table of α versus g. In the limit of large g, $\alpha \approx 1 - 1/g$. Our first estimate of a (call it a') can then be determined by using the EES approach to determine that a' gives the correct $\langle\lambda_{r1}\rangle$. At this point, we have a chain with the correct $\langle\lambda_{r1}\rangle$ as well as $\langle\lambda_{r2}\rangle$, but $\langle\lambda_{r3}\rangle$ is probably incorrect. Consider now the equation

$$\begin{pmatrix} \langle\lambda_{r1}\rangle - \langle\lambda_{r1}\rangle' \\ \langle\lambda_{r2}\rangle - \langle\lambda_{r2}\rangle' \\ \langle\lambda_{r3}\rangle - \langle\lambda_{r3}\rangle' \end{pmatrix} = \begin{pmatrix} \frac{\partial\langle\lambda_{r1}\rangle}{\partial a} & \frac{\partial\langle\lambda_{r1}\rangle}{\partial b_0} & \frac{\partial\langle\lambda_{r1}\rangle}{\partial g} \\ \frac{\partial\langle\lambda_{r2}\rangle}{\partial a} & \frac{\partial\langle\lambda_{r2}\rangle}{\partial b_0} & \frac{\partial\langle\lambda_{r2}\rangle}{\partial g} \\ \frac{\partial\langle\lambda_{r3}\rangle}{\partial a} & \frac{\partial\langle\lambda_{r3}\rangle}{\partial b_0} & \frac{\partial\langle\lambda_{r3}\rangle}{\partial g} \end{pmatrix} \begin{pmatrix} a - a' \\ b_0 - b_0' \\ c - c' \end{pmatrix} \tag{6}$$

which can be written in compact notation as

$$\Lambda = A\delta \tag{7}$$

where unprimed/primed quantities correspond to correct/approximate values. The **A** matrix is determined by using the EES method on three additional chains (with $a' + \Delta a$, b', g', and so on) and then evaluating the partial derivatives. What we actually need to determine is δ which requires straightforward inversion of a 3 × 3 matrix

$$\delta = A^{-1}\Lambda \tag{8}$$

If fairly large changes in the initial chain parameters are required, it may be necessary to reevaluate **A** since the elements depend on a, b_0, and g. In summary, one first derives an approximate chain with parameters a', b_0', and g'. Then **A** and its inverse are computed and the new parameters calculated according to eq 8. The new parameters, in turn, are checked by application of the EES method to the reparametrized chain.

Simulation of Electric Birefringence or Dichroism. In order to simulate a particular dynamics experiment, it is necessary to average some appropriate quantity over an ensemble of different structures as they evolve in time. The Brownian dynamics approach based on the Ermak–McCammon algorithm,[37] which carries out a single trajectory, has been described in detail previously.[40,55] In this work, a dynamics time step, Δt, between 0.10 ns (for HZ chains) and 2.5 ns (for a 10 subunit chain model of 367 bp DNA) is used depending on the system. Basically, Δt must be chosen sufficiently small so that position-dependent quantities like stretching and bending forces do not change significantly during Δt. At regular time intervals during a trajectory, t', which can be called the sampling interval, a reduced birefringence or dichroism decay is computed. At sample time lt', we compute for a range of m

$$H_s(lt',mt') = \frac{1}{(N-1)^2}\sum_{ik} P_2[\cos(\mathbf{u}_i(mt')\cdot\mathbf{u}_k(lt'))] \tag{9}$$

$$H_i(lt',mt') = \frac{1}{(N-1)^3}\sum_{ijk} P_1[\cos(\mathbf{u}_i(mt')\cdot\mathbf{u}_j(mt'))]\, P_2[\cos(\mathbf{u}_j(mt')\cdot\mathbf{u}_k(lt'))] \tag{10}$$

where P_x is the Legendre polynomial of rank x and $\mathbf{u}_i(mt')$ is the unit vector along the ith virtual bond at time t'. The s and i subscripts on H refer to saturation-induced (eq B16) and induced (eq B24) electric dipole orienting mechanisms. In eqs 9 and 10, l is an integer which ranges from 1 to n where n is the final sampling interval (usually set to 200–1000) of a particular trajectory. The total number of intervals considered in computing EB or ED decays, n^*, isless than or equal to n (set to 100 in this work). The range of m in eqs 9 and 10 is from 0 (if $l < n^*$) or $l - n^*$ ($l \geq n^*$) to l. Assuming the applied field is small enough that it does not distort the macromolecule, then EB or ED decay can be evaluated as a stationary quantity[57] and the following average is computed

$$\langle H_x(qt')\rangle_t = \frac{1}{(n-q)}\sum_{k=1}^{n-q} H_x((k+q)t',kt') \tag{11}$$

where x refers to s or i, the t subscript denotes a time average over a single trajectory, and q ranges from 0 to $n^* - 1$. This procedure is repeated for an "ensemble" of 30–300 trajectories in the present work depending on n. The final EB or ED reduced decay, which has an initial amplitude of 1, can be written as

$$g_x(qt') = \langle\langle H_x(qt')\rangle_t\rangle_e \tag{12}$$

where the e subscript refers to an ensemble average. A

major advantage in setting $n \gg n^*$ is that the noise level in eq 12 is more uniform over the entire q range. Despite the fact that a long trajectory requires more CPU than a shorter one, more configurations are sampled at the long time end and, hence, fewer trajectories per simulation must be carried out. The reproducibility of $g_x(t)$ is checked by examining variations in four equivalent but independent subsimulations which, taken together, comprise the overall simulation.

The reduced decays are analyzed using CONTIN developed by Provencher and co-workers.[43] This is a versatile, model-independent data analysis program which fits $g_x(t)$ to a continuous distribution of relaxation times

$$g_x(t) = \int_0^\infty G_x(\tau)e^{-t/\tau}\,dt \qquad (13)$$

where $G_x(\tau)$ is a normalized distribution function and τ is a relaxation time. In general, this is an ill-posed problem since many possible solutions exist that fit the data within experimental error. In CONTIN, the problem is formulated as a weighted least-squares fit with an added quadratic term called the regularizer which favors simpler, "smoother" solutions. The application of this program to dynamic light scattering[55] and electric birefringence[11,29] has been discussed before. In this work, reproducibility of the $G_x(t)$'s is checked by (1) adding different Gaussian random noise backgrounds (with standard deviations comparable to those between subsimulations) to $g_x(t)$ and seeing how this affects $G_x(\tau)$ and (2) comparing $G_x(\tau)$'s for identical but independent simulations. The $G_x(\tau)$'s reported here represent CONTIN "chosen solutions".

In addition to flexible chains, ED/EB decays from rigid chains are also of interest. Although these could be obtained from by Brownian dynamics simulation using a rigid-body algorithm,[58] it is more efficient in the present work to use the equations of Wegener and co-workers[59] for the ED/EB decay of arbitrary rigid bodies. As discussed previously,[29] the EES approach and Wegener's equations are used to calculate birefringence decays from an ensemble of rigid chains. This algorithm offers the additional advantage that the distribution of relaxation times can be obtained explicitly.

III. Results

Evaluation of the Equivalent Chain Approach and Analysis by CONTIN. The ability of a simple "equivalent" chain to mimic the actual birefringence decay of a more realistic HZ model chain can be directly demonstrated for rigid ensembles. Briefly, a structure is selected from an equilibrium ensemble and its transport properties are determined. Using rigid-body equations,[59] the birefringence decay is computed as a sum of exponentials. For 194 bp DNA with $P = 50$ nm, the reduced decay of a sample chain consists of three relaxation times; $\tau = 0.48$, 1.25, and 3.70 μs, with amplitudes 0.09, 0.02, and 0.89, respectively. Different chains have different amplitudes and lifetimes because of variation in conformation. In general, the decay consists of up to five relaxation times for arbitrary rigid bodies, but this simplifies to three distinct ones in the present case since the smallest two rotational eigenvalues are nearly equal ($\lambda_{r1} \approx \lambda_{r2} \equiv D_\perp$). The largest lifetime component has $\tau_0 = 1/(6D_\perp)$ and corresponds to pure end-over-end rotational diffusion. The two faster times are given by $\tau_1 = 1/(5D_\perp + D_\parallel)$ and $\tau_2 = 1/(2D_\perp + 4D_\parallel)$ where $\lambda_{r3} = D_\parallel$.[59] They represent more complex combinations of both end-over-end and more rapid axial tumbling motions. Nonetheless it should be emphasized that all three relaxation times represent overall rotational motions. By superimposing the amplitude versus lifetime histograms of several hundred chains, $G_s(\tau)$ can be generated. The s subscript refers to an assumed SID orienting mechanism. An example is shown in Figure 1 for 194 bp DNA with $P = 50$ nm for 21 subunit HZ (squares) and 10 subunit equivalent chains (+'s). It is clear from the figure that the equivalent chain accurately reproduces the birefringence decay of the more detailed model, at least as far as rigid structures are concerned. From the previous discussion, we can identify the long-time, large-amplitude peak as corresponding to pure end-over-end rotational diffusion and the shorter time, small-amplitude peak as corresponding to combined end-over-end and axial tumbling motions. Note that, upon taking the ensemble average, the two faster times coalesce to give a single rather broad lifetime distribution.

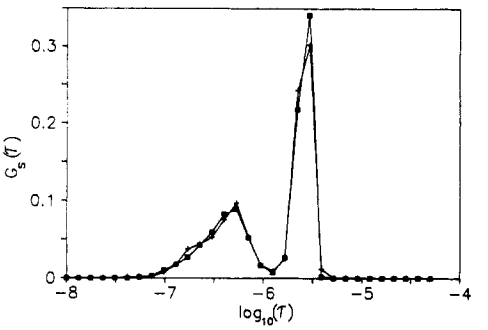

Figure 1. Lifetime distribution for rigid 194 bp DNA fragments with $P = 50$ nm. Filled squares and pluses correspond to 21 (HZ) and 10 subunit chains, respectively. τ is in seconds. The assumed orienting mechanism is SID for this figure as well as Figures 2–8.

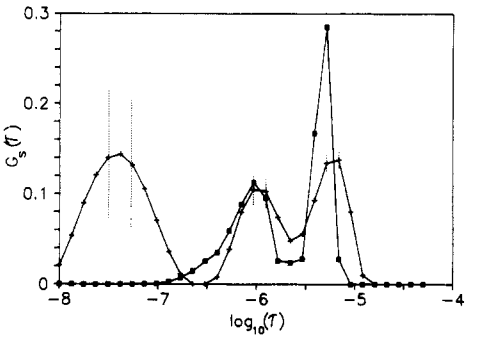

Figure 2. Lifetime distribution for rigid 250 bp DNA fragments with $P = 50$ nm. Filled squares and pluses correspond to actual and CONTIN distributions, respectively. Dotted vertical lines on select points denote error limits in the CONTIN distribution.

In the analysis of flexible-chain simulations, we are unable to determine the lifetime distribution directly and have to resort to indirect methods such as that provided by CONTIN. The rigid ensemble studies allow us to determine how accurately CONTIN reproduces the actual distribution, and this is illustrated in Figure 2 for 250 bp DNA with $P = 50$ nm. The actual lifetime distribution is given by the squares and that estimated by CONTIN is given by the +'s. The latter distribution was obtained by first computing the ensemble-averaged birefringence decay followed by CONTIN analysis. The two long-time peaks are fairly well reproduced but shifted to slightly longer times. For consistency sake, all rigid ensemble lifetime and amplitude data reported in the remainder of this work come from CONTIN analyses rather than from the actual distributions. The shortest CONTIN peak (with a lifetime less than 0.1 μs) is clearly spurious in this case and occurs on a time scale comparable to the shortest sampling time interval used in constructing the correlation function. Short-time components like this are frequently seen in CONTIN analyses and contribute less than 1% to the decay

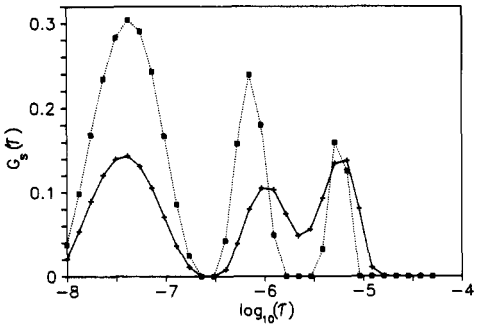

Figure 3. Effect of flexibility on CONTIN lifetime distributions. Filled squares and pluses correspond to flexible and rigid chains, respectively. The case illustrated corresponds to a 250 bp fragment with P = 50 nm.

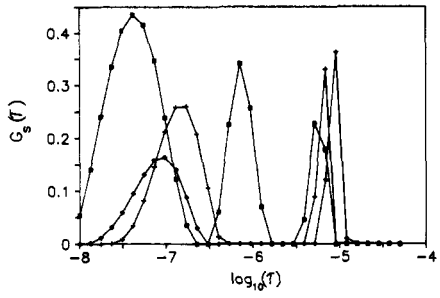

Figure 4. CONTIN distribution for flexible 250 bp DNA for different persistence lengths, P. Filled squares, pluses, and diamonds correspond to P = 50, 100, and 200 nm, respectively.

amplitude. Note also the much higher level of error in the fastest peak. Because of their irreproducibility and low amplitude, they shall be ignored.

The effect of chain flexibility on the lifetime distribution is shown in Figure 3 for 250 bp DNA with P = 50 nm. Again an SID orienting mechanism is assumed. The CONTIN rigid distribution (+'s) of Figure 2 is shown along with the corresponding flexible distribution (squares) derived from Brownian dynamics simulation. Basically, a_0 and a_1 are comparable in both cases, but τ_0 and τ_1 are reduced by about 10% and 30%, respectively, when the chains are allowed to flex. (The a's and τ's correspond to amplitudes and peak first moments of the lifetime distribution which are printed out by the CONTIN program.) Figure 4 shows how the lifetime distribution of flexible 250 bp DNA depends on P for P = 50 (squares), 100 (+'s), and 200 nm (diamonds). Note that τ_0 increases as P increases but that τ_1 shows the opposite trend. Also, a_1 decreases as P increases. First moment amplitudes (a's) and lifetimes (τ's) are summarized in Table I for these and other cases. Since it can be argued that assigning a distribution is tantamount to overinterpreting the data, emphasis in the remainder of this work will be placed on the a's and τ's.

The validity of the equivalent chain approach with regards to flexible structures can be evaluated by looking at different equivalent chains with variable subunit number and seeing how the amplitudes and lifetimes vary with N. This is shown in Table II for 194 bp DNA with P = 50 nm for N ranging from 5 to 21 (N = 21 corresponds to a HZ model). Numbers in parentheses represent variations seen in independent simulations and approximate standard deviations. It is clear from this table that the N = 10 and 21 results are indistinguishable within the resolution of the data. Consequently, we can conclude that the 10 subunit chain is detailed enough to reproduce the ED/EB decay of the more realistic HZ chain.

Longest and First Internal Times versus Chain Length. Diekmann and co-workers[13] have carried out high-field electric dichroism (ED) experiments on short DNA fragments in the size range 100–250 bp. Fitting their data to a double-exponential decay, they observed that, although the relative amplitude of the fast component increases as the field strength increases, both lifetimes are essentially independent of field strength. Because of this, it is not unreasonable to compare the lifetimes of Diekmann et al. with simulated values and also those from low-field electric birefringence (EB) experiments reported by Lewis et al.[11] Plotted in Figure 5 are τ_0's from Diekmann et al. (squares) and Lewis et al. (+) along with simulations on P = 50 nm chains for rigid (diamonds) and flexible (triangles) chains. The SID orienting mechanism has been assumed in these particular simulations. Simulation results bracket fairly well experimental values with

Table I
Comparison of ED/EB Results Based on Induced (I) and Saturation-Induced (S) Orienting Dipole Mechanisms

bp	P, nm	orientation mechanism	a_0	a_1	τ_0, μs	τ_1, μs
194	50	S	0.85 (0.02)	0.15 (0.02)	3.3 (0.2)	0.30 (0.03)
194	50	I	0.83 (0.01)	0.16 (0.01)	3.7 (0.1)	0.37 (0.07)
250	50	S	0.78 (0.03)	0.18 (0.02)	5.7 (0.3)	0.84 (0.15)
250	50	I	0.80 (0.02)	0.15 (0.02)	6.3 (0.2)	0.93 (0.20)
250	100	S	0.93 (0.01)	0.07 (0.01)	7.3 (0.4)	0.30 (0.08)
250	100	I	0.93 (0.01)	0.07 (0.01)	7.2 (0.2)	0.32 (0.02)
250	200	S	0.98 (0.01)	0.02 (0.01)	8.5 (0.1)	0.11 (0.04)
250	200	I	0.97 (0.01)	0.03 (0.01)	8.6 (0.2)	0.21 (0.05)
367	50	S	0.66 (0.02)	0.27 (0.03)	13.2 (0.5)	1.73 (0.05)
367	50	I	0.76 (0.05)	0.20 (0.01)	13.7 (0.3)	1.62 (0.05)
367	100	S	0.84 (0.01)	0.13 (0.02)	18.5 (0.5)	1.44 (0.10)
367	100	I	0.88 (0.02)	0.20 (0.05)	17.9 (0.8)	1.00 (0.10)
367	200	S	0.96 (0.01)	0.04 (0.01)	21.3 (0.3)	0.68 (0.16)
367	200	I	0.94 (0.01)	0.06 (0.01)	22.9 (0.7)	1.10 (0.10)

Table II
Amplitudes and Lifetimes for Flexible 194 Base-Pair DNA, P = 50 nm

N	a_0	τ_0, μs	a_1	τ_1, μs
5	0.83 (0.02)	3.61 (0.20)	0.15 (0.03)	0.39 (0.03)
10	0.85 (0.02)	3.30 (0.20)	0.15 (0.02)	0.30 (0.03)
21 (HZ)	0.89 (0.03)	3.23 (0.15)	0.11 (0.03)	0.33 (0.10)

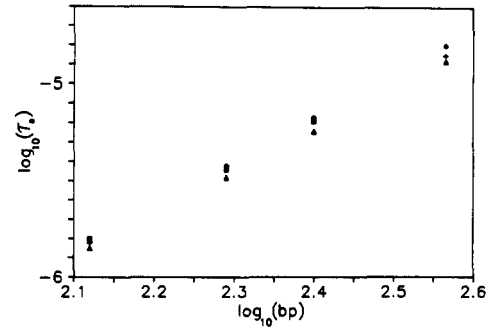

Figure 5. Longest relaxation time versus fragment length. Filled squares and pluses correspond to ED and EB experiments, respectively. Diamonds and triangles correspond to rigid and flexible simulations with P = 50 nm.

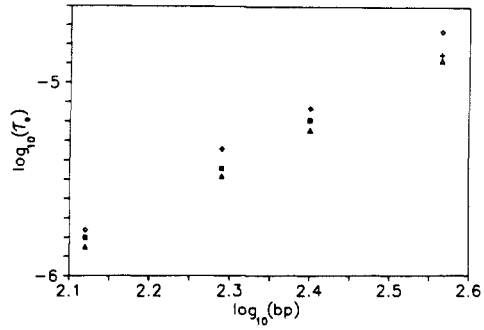

Figure 6. Similar to Figure 5. Diamonds and triangles correspond to flexible simulations with P = 100 and 50 nm, respectively.

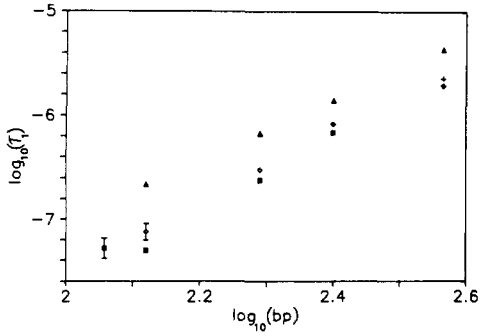

Figure 7. First internal time versus fragment length. Filled squares and pluses correspond to ED and EB experiments, respectively. Diamonds and triangles correspond to rigid and flexible simulations with P = 50 nm.

the rigid-chain lifetimes consistently longer than the corresponding flexible values. It is worth noting that the EB results on 367 bp DNA (+) fall close to a least-squares fit through the ED data points despite differences in field strengths and data analysis in the two sets of experiments. As in the present study, Lewis et al. analyzed their data using CONTIN. When simulated data are fit to a double-exponential decay, amplitudes and lifetimes are obtained which are in good agreement with those derived from CONTIN. Plotted in Figure 6 are simulation results (SID orienting mechanism) on flexible chains with P = 50 nm (triangles) and 100 nm (diamonds) along with experimental τ_0's. Modeling the DNA as a flexible wormlike chain, a value of P between 50 and 100 nm is consistent with all fragments. However, modeling the DNA as a rigid wormlike chain results in an inferred value that is slightly lower than 50 nm.

The dependence of the first internal time, τ_1, on chain length for P = 50 nm rigid (triangles) and flexible (diamonds) model chains is shown in Figure 7. As before ED and EB values are denoted by filled squares and +'s, respectively. It is clear from this figure that τ_1's for the rigid model are substantially longer than flexible and experimental lifetimes. Flexible τ_1's are slightly longer than those observed experimentally except for the 367 bp fragment. Increasing P would reduce τ_1 and improve overall agreement between simulation and experiment, which is also entirely consistent with the behavior of τ_0. The effect of P on τ_1 for flexible-chain models is shown in Figure 8 with P = 50, 100, and 200 nm corresponding to diamonds, triangles, and crosses, respectively.

At this point, it is worthwhile to summarize the results of Figures 5–8. A rigid model with $P \approx 50$ nm is quite consistent with the chain-length dependence of τ_0 observed experimentally. The same model, however, is not at all consistent with experiments with regards to τ_1. A flexible wormlike chain which uses a simple harmonic bending

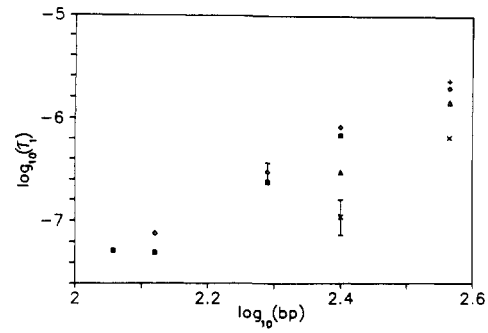

Figure 8. Similar to Figure 7. Diamonds, triangles, and crosses correspond to flexible simulations with P = 50, 100, and 200 nm, respectively.

potential is quite consistent with both τ_0 and τ_1 for the size range 100–367 bp for a persistence length slightly larger than 50 nm. This finding is at odds with that of Song and Schurr,[36] who concluded that a dynamic persistence length of 200 nm is required in order to account for the magnitude of τ_1 and its dependence on chain length. We feel the reason for this discrepancy lies in the average used to compute the ED decay. Song and Schurr used an equation similar to eq B16, but the double sum over i and k is replaced by a single sum (over i). This average is appropriate for the fluorescence polarization anisotropy of a chromophore bound tightly and randomly to a linear chain molecule[60] but is not appropriate for low-field ED or EB decay. It does, however, raise the important point that similar experiments which monitor different dynamical averages can have quite different relaxation time spectra.

As discussed in the Introduction the saturation-induced dipole mechanism is not appropriate at low field such as used in the birefringence experiments of Eden and coworkers.[9,11,29] At low fields, an induced dipole orienting mechanism would be more appropriate. In the case of an induced dipole mechanism, the appropriate average is given by eq B24. Summarized in Table I are lifetimes and amplitudes for a number of different wormlike chains for both induced (I) and saturation-induced (S) dipole orienting mechanisms. Despite small differences, we can conclude the two orienting mechanisms yield similar relaxation time spectra both with regards to lifetime and amplitude.

IV. Conclusions

The ED/EB off-field decay of DNA fragments in the size range 100–367 bp consists basically of two relaxation processes. The larger amplitude, slower decay process is fairly insensitive to chain flexibility, and its lifetime is reduced by about 10% when bending motions are allowed. Using rigid-body models to infer persistence lengths from the longest relaxation time of ED/EB measurements is reasonably accurate but results in an underestimation of P. The smaller amplitude, faster decay process is much more sensitive to chain flexibility. It is not possible to find rigid model chains which are consistent with experimental τ_0 and τ_1 values simultaneously. However, a simple elastic bending wormlike chain with $P \approx 50$ nm is consistent with experimental lifetimes for all lengths in the range studied. This of course does not prove that DNA bends as a simple elastic body, but it does show that this model is consistent with ED/EB measurements.

The model simulations carried out in this work are approximate in several respects. To begin with, the chain model employed preserves only the global details of DNA fragments they are supposed to represent. Nonetheless,

test studies on both rigid and flexible chains in which the number of subunits is varied demonstrate that the 10 subunit equivalent chains used in most of this work are detailed enough to model ED/EB decay on the 131–367 bp DNA fragments. A coupling between torsion and bending motions might also be expected to influence EB/ED decay. In a preliminary study, torsion was also included in a few simulations and the dependence of the relevant correlation functions on torsional rigidity examined with other parameters held constant.[35] Within the uncertainty of the data, no dependence of EB/ED decay on torsional rigidity was observed, and in all subsequent work the torsional rigidity was set to a low value and ignored. This conclusion, however, is only tentative since the torsion model as described is ref 35 is restricted to chains in which the angle between adjacent virtual bonds is close to zero. Although this condition is satisfied for "detailed" chains made up of touching subunits, it is probably not meaningful to apply it to a 10 subunit chain equivalent to a 367 base-pair DNA fragment with $P = 50$ nm for example. As discussed in the Introduction, the orientation mechanism for polyelectrolytes in external fields remains poorly understood. In this work, ED/EB decay from the two extreme mechanisms of purely induced and saturation-induced electric dipole moments has been considered. We have shown that lifetimes and amplitudes for both mechanisms are about the same, which suggests that ED/EB decay is fairly insensitive to the way the chain is oriented at least at low field strengths which the present results are strictly limited to.

It is clear from the measurements of Diekmann et al. that the external field strength does influence ED decay but that the effect is restricted primarily to the amplitudes rather than to the lifetimes of the decay processes. For that reason, we have focused attention in this work to the decay lifetimes in comparing simulations and experiments. It would be possible to extend the simulations to high electric fields by using Monte Carlo methods to first orient the fragment and then investigate the transient decay of an ensemble of fragments. Considering the field-strength dependence of ED/EB decay amplitudes from such studies would undoubtedly help us understand better the orientation mechanisms of DNA and other polyelectrolytes. We plan to pursue this line of investigation in the future.

Acknowledgment. S.A.A. acknowledges the donors of the Petroleum Research Fund, administered by the American Chemical Society, for partial support of this research. Professors J. Michael Schurr and Bruce Robinson also deserve thanks for useful discussions and for providing much of the stimulus for this study.

Appendix A

In order to relate the transient electric birefringence or dichroism (TEB or TED) decay measurement of a linear polyion to a model-dependent correlation function, it is necessary to know the probability, $w(\phi_0)$, that the chain is in a particular configuration, ϕ_0, at the time the orienting electric field is turned off. This probability distribution is related to the electrostatic potential energy of the polyion, $V(\phi_0)$, by

$$w(\phi_0) = A\langle \exp(-\beta V(\phi_0))\rangle \tag{A1}$$

where $\beta = 1/k_B T$, A is a normalization constant, and brackets denote an ensemble average. Consider first the case in which the polyion is oriented by a purely induced dipole mechanism. In this case

$$V(\phi_0) = -\frac{1}{2}\mathbf{E}\cdot\chi\cdot\mathbf{E} \tag{A2}$$

where $\mathbf{E}$ is the applied electric field and χ is the electric polarizability tensor of the polyion. At low fields, χ is related to the instantaneous dipole moment, $\mathbf{p}$, by

$$\chi = \beta\langle \mathbf{p}\mathbf{p}^{\mathrm{T}}\rangle \tag{A3}$$

where T denotes transpose of, in this case, a column vector and brackets denote a time average long compared to fluctuations in $\mathbf{p}$ but short compared to overall reorientations of the macromolecule. Oosawa[54] considered a simple model by equating $\mathbf{p}$ to $q\mathbf{d}$ where q is an effective charge of the polyion and $\mathbf{d}$ the instantaneous displacement between the centers of the polyion and counterion charge distributions. In the present work, we shall use Oosawa's basic idea but generalize it to make it compatible to our model of a linear macroion made up of N subunits connected by $N-1$ virtual bonds, $\mathbf{b}_j$. The relationship of the virtual bond or subunit to the actual polymer is somewhat arbitrary. It could represent, for example, one monomer unit of the chain. The net dipole moment is written as the sum over $N-1$ virtual bond dipole moments.

$$\mathbf{p} = \sum_i q_i \mathbf{b}_i \tag{A4}$$

The assumption is made that the virtual bond and virtual bond dipole moments are collinear. On a time scale short compared to coil deformations, eq A3 becomes

$$\mathbf{p} = \beta \sum_{ij} \mathbf{b}_i \mathbf{b}_j^{\mathrm{T}} \langle q_i q_j\rangle \tag{A5}$$

Consider the special case of a rodlike or nearly rodlike polyion in which we make our basic unit size small (large N). This would be appropriate, for example, if we had a DNA fragment much shorter than a persistence length and the basic unit is taken as a base pair. In that case, all of the $\mathbf{b}_i$'s are equal and eq A5 can be written

$$\chi = \beta \mathbf{b}\mathbf{b}^{\mathrm{T}} \sum_{ij} \langle q_i q_j\rangle \tag{A6}$$

If charge fluctuations are weakly correlated, it can be seen that χ should vary linearly with N or the polyion molecular weight, M. If, on the other hand, charge fluctuations are strongly correlated ($\langle q_i q_j\rangle$ = constant), then eq A6 predicts a M^2 dependence on χ. For DNA, which is the polyion of interest in this work, the electric polarizability varies roughly as M^2, which means that the strongly correlated case is appropriate. Thus, eq A5 can be written as

$$\chi = \frac{\alpha}{(N-1)^2} \sum_{ij} \mathbf{u}_i \mathbf{u}_j^{\mathrm{T}} \tag{A7}$$

where the $\mathbf{u}$'s are the virtual bond unit vectors and α is a constant. This form of χ is different from that used previously[29] in which a simple sum over virtual bond polarizabilities was taken. The basic problem with that model is that it predicts the incorrect length dependence of χ. Combining eqs A1, A2, and A9 then yields

$$w(\phi_0) = A\left\langle \exp\left[+ \frac{\beta\alpha E^2}{2(N-1)^2} \sum_{ij} \cos\theta_{i0} \cos\theta_{j0} \right] \right\rangle \tag{A8}$$

where θ_{i0} is the angle between virtual bond i at $t = 0$ and the applied field.

As discussed in the Introduction, the induced dipole of DNA appears saturated at fairly low field strengths. When

steady-state electric dichroism or birefringence measurements on a range of different monodisperse DNA fragments (100–300 bp) are interpreted in terms of saturation-induced dipole (SID) models, a critical field strength, E_0, of between 3 and 10 kV/cm is deduced.[49,50] Also, E_0 appears to decrease with increasing fragment size. Thus eq A8 may be appropriate for the low-field TEB experiments of Eden and co-workers[9,11,29] but not the TED experiments of Diekmann et al.[12,13] where field strengths in the range 10–50 kV/cm were used.

To account for dipole saturation in an approximate way, we shall use essentially the SID model modified to accommodate our multisubunit polyion. Start by first considering the dipole moment, $\mathbf{p}$, of a macromolecule in a small external field directed along z using eq A7

$$\mathbf{p} = \chi\cdot\mathbf{E} = \frac{\alpha E}{(N-1)^2}\left(\sum_i \mathbf{u}_i\right)\left(\sum_j u_{jz}\right) \tag{A9}$$

In the original SID model,[48,49] u_{jz} in eq A9 above is replaced by $\pm E_0/E$ if $|\mathbf{u}_j\cdot\mathbf{E}|$ exceeds E_0 and the + or − sign is taken if u_{jz} is positive or negative. Here we shall make the two simplifying assumptions that E_0 is sufficiently small that conformations with $|\mathbf{u}_j\cdot\mathbf{E}|$ less than E_0 can be ignored and that all u_{jz}'s of a chain in a given conformation are simultaneously positive or negative. The latter assumption is strictly valid for a rodlike polyion. In this case, eq A9 can be written

$$\mathbf{p} = \pm\frac{\alpha E_0}{(N-1)}\sum_i \mathbf{u}_i \tag{A10}$$

where the + (−) sign is taken if the projection of the end-to-end vector on the field direction is positive (negative). For this model, $V(\chi_0) = -\mathbf{p}\cdot\mathbf{E}$ and

$$w(\phi_0) = A\exp\left[+\frac{\beta\alpha E_0 E}{(N-1)}\sum_i |\cos\theta_{i0}|\right] \tag{A11}$$

Appendix B

The objective of this appendix is to show that the electric birefringence or dichroism decay is given by eqs 9 and 10 in the text when the applied field strength is small. In what follows, we shall restrict ourselves to electric dichroism keeping in mind that an entirely analogous derivation would follow for the case of birefringence. It shall be assumed that an electric field, $\mathbf{E}$, is applied to the sample in the z direction for a length of time long enough for the macromolecules to achieve a steady orientation. At time $t = 0$, the field is turned off and the dichroism decay, $\Delta A(t)$, is measured

$$\Delta A(t) = A_z(t) - A_x(t) = cl\langle a_z(t) - a_x(t)\rangle \tag{B1}$$

where $A_\alpha(t)$ is the absorption of the sample in the α direction at t, c is the concentration of macromolecule, l is the pathlength, and $\langle a_\alpha(t)\rangle$ is the average absorption cross section in the α direction for a single macromolecule at time t. It shall be assumed that the macromolecule is made up of $N-1$ identical absorbing chromophores. (In the case of birefringence, the assumption is made that the optical polarizability of the macromolecule is the tensor sum over $N-1$ identical virtual bond polarizabilities.) We can then write

$$\langle\Delta a(t)\rangle = \sum_k \langle\Delta a_k(t)\rangle \tag{B2}$$

where Δa_k is the dichroism of the kth subunit. Each term in eq B2 can be written as an average over internal configurations of the molecule

$$\langle\Delta a_k(t)\rangle = \int d\phi\, w(\phi,t)\,\Delta a(\Omega_k) \tag{B3}$$

where ϕ denotes a particular configuration of the macromolecule in the lab frame, $w(\phi,t)$ is the probability the macromolecule is in configuration ϕ at time t, and $\Delta a(\Omega_k)$ is the dichroism of a subunit in configuration Ω_k. It should be emphasized that Ω_k is a subset of ϕ. Equation B3 can also be written

$$\langle\Delta a_k(t)\rangle = \int d\phi\, d\phi_0\, w(\phi_0)\, G(\phi,t|\phi_0)\,\Delta a(\Omega_k) \tag{B4}$$

where $w(\phi_0)$ is the probability the macromolecule is in configuration ϕ_0 at $t = 0$ and $G(\phi,t|\phi_0)$ is the conditional probability the macromolecule is in configuration ϕ at time t given that it is in ϕ_0 at $t = 0$.

At this stage, it will be convenient to write $\Delta a(\phi_k)$ in terms of spherical tensors

$$a_z(\Omega_k) = a_{00} + \frac{2}{3}a_{20}(\Omega_k) \tag{B5}$$

$$a_x(\Omega_k) = a_{00} - \frac{1}{3}a_{20}(\Omega_k) + \frac{1}{\sqrt{6}}(a_{22}(\Omega_k) + a_{2-2}(\Omega_k))$$

where a_{lm} is the mth component of a spherical tensor of rank l. Since a_{00} is orientationally invariant, it is independent of Ω_k. Spherical tensors transform under rotation as[61]

$$a_{lm}(\Omega_k) = \sum_n D^l_{nm}(bL)\, a_{ln}(\Omega'_k) = \sum_n D^{l*}_{mn}(Lb)\, a_{ln}(\Omega'_k) \tag{B6}$$

where the D denotes Wigner rotation matrices, (bL) is the Euler transformation which carries some convenient body fixed reference frame, b, into the laboratory frame, L, and Ω'_k is the configuration of subunit k in the b frame. (In the second entry of eq B6, the Euler transformation has been inverted.) Thus we can write

$$\Delta a(\Omega_k) = \sum_n a_{2n}(\Omega'_k)\left[D^{2*}_{0n}(Lk_0) - \frac{1}{\sqrt{6}}D^{2*}_{2n}(Lk_0) - \frac{1}{\sqrt{6}}D^{2*}_{-2n}(Lk_0)\right] \tag{B7}$$

where we have chosen the b frame to correspond to a body fixed frame associated with subunit k at time 0. Note from eq B7 that $\Delta a(\Omega_k)$ transforms as a second rank irreducible tensor.

Assuming the absorption cross section is $a_\parallel$ and $a_\perp$ parallel and perpendicular to a virtual bond, we can write

$$a_{2n}(\Omega'_k) = D^2_{0n}(kk_0)\Delta a \tag{B8}$$

where $\Delta a = a_\parallel - a_\perp$ and we have chosen the z axis of the b frame to lie along virtual vector k at time 0. It will also prove convenient to transform the $D^{2*}_{mn}(Lk_0)$ terms in eq B7 to a body fixed frame associated with bond i at $t = 0$ using the transformation property[61]

$$D^l_{nm}(ab) = \sum_s D^l_{ns}(ac)\, D^l_{sm}(cb) \tag{B9}$$

Making use of eqs B8 and B9 in eq B7 yields

$$\Delta a(\Omega_k) = \Delta a \sum_n D^2_{0n}(kk_0) \sum_m D^{2*}_{mn}(i_0k_0) \left[D^{2*}_{0m}(Li_0) - \frac{1}{\sqrt{6}} D^{2*}_{2m}(Li_0) - \frac{1}{\sqrt{6}} D^{2*}_{-2m}(Li_0) \right] \quad \text{(B10)}$$

From eqs A11 and A8 we can write

$$w_s(\phi_0) = A\left[1 + \frac{\beta\alpha E_0 E}{(N-1)} \sum_i |D^1_{00}(Li_0)| \right] \quad \text{(B11)}$$

for the saturation-induced dipole (SID) model and

$$w_i(\phi_0) = A\left[1 + \frac{\beta\alpha E^2}{2(N-1)^2} \sum_{ij} D^1_{00}(Li_0) D^1_{00}(Lj_0) \right] \quad \text{(B12)}$$

for the induced dipole (ID) model. In both eqs B11 and B12, the exponentials have been expanded and only the leading terms retained. Consider first the evaluation of $\langle \Delta a_k(t) \rangle$ for the SID model using eqs B4, and B10 and B11. The unit term vanishes in eq B11 so we can write

$$\langle \Delta a_k(t) \rangle = \frac{\beta\alpha E_0 E A \Delta a}{(N-1)} \sum_{inm} \int d\phi' \int d\phi_0' \, G(\phi' t|\phi_0') D^2_{0n}(kk_0) \, D^{2*}_{mn}(i_0k_0) \, d\Gamma \, |D^1_{00}(Li_0)| \left[D^{2*}_{0m}(Li_0) - \frac{1}{\sqrt{6}} D^{2*}_{2m}(Li_0) - \frac{1}{\sqrt{6}} D^{2*}_{-2m}(Li_0) \right] \quad \text{(B13)}$$

where $d\Gamma$ represents the differential volume element for the Euler transformation (Li_0), and primes denote that the reference frame is now taken with respect to subunit i at $t = 0$. Because the bonds are assumed cylindrically symmetric, only the first two Euler angles are needed to specify (Li_0) or (i_0j) for that matter. In evaluating the integral over $d\Gamma$, both D^{2*}_{2m} and D^{2*}_{-2m} (Li_0) terms vanish. In addition, most of the m terms vanish since subsequent averaging over the (i_0k_0) transformation eliminates all $m \neq 0$ terms. Now it is straightforward to show

$$\int d\Gamma \, |D^1_{00}(Li_0)| D^{2*}_{00}(Li_0) = \pi/2 \quad \text{(B14)}$$

In addition, since only first-order terms are being retained, it turns out $A = 1/4\pi$. Thus, eq B13 can be written as

$$\langle \Delta a_k(t) \rangle = \frac{\beta\alpha E_0 E \Delta a}{8(N-1)} \sum_{in} \int d\phi' \, d\phi_0' \, G(\phi' t|\phi_0') \, D^2_{0n}(kk_0) \times D^{2*}_{0n}(i_0k_0) \quad \text{(B15)}$$

Using the identity $D^{l*}_{mn}(ab) = D^l_{nm}(ba)$ along with eq B9 and summing over k yields finally

$$\langle \Delta a(t) \rangle = \frac{\beta\alpha E_0 E \Delta a}{8(N-1)} \sum_{ik} \langle D^2_{00}(ki_0) \rangle \quad \text{(B16)}$$

The average in eq B16 is independent of the initial orientation of the macromolecule in the applied field and depends only on internal coordinates. Internal averages like this one are readily evaluated by Brownian dynamics simulation.

For the induced dipole mechanism, the averaging procedure is different. As in the SID case, the unit term in eq B12 vanishes on subsequent averaging and $A = 1/4\pi$. We can write

$$w_i(\phi_0) = \frac{\beta\alpha E^2}{8\pi(N-1)^2} \sum_{ij} D^1_{00}(Li_0) \, D^1_{00}(Lj_0) = \frac{\beta\alpha E^2}{8\pi(N-1)^2} \sum_{m_1m_2} D^1_{0m_1}(Lk_0) \, D^1_{0m_2}(Lk_0) \sum_{ij} D^1_{m_10}(k_0i_0) \times D^1_{m_20}(k_0j_0) = \frac{\beta\alpha E^2}{8\pi(N-1)^2} \sum_{lm_1m_2} C(11l;00) \times C(11l;m_1m_2) \, D^l_{0,m_1+m_2}(Lk_0) \sum_{ij} D^1_{m_10}(k_0i_0) \, D^1_{m_20}(k_0j_0) \quad \text{(B17)}$$

where use has been made of the contraction relation[61]

$$D^p_{ij} D^q_{mn} = \sum_r C(pqr;im) \, C(pqr;jn) \, D^r_{i+m,j+n} \quad \text{(B18)}$$

Multiplying eq B17 with $\Delta a(\Omega_k)$

$$\Delta a(\Omega_k) = \Delta a \sum_n D^2_{0n}(kk_0) \left[D^{2*}_{0n}(Lk_0) - \frac{1}{\sqrt{6}} D^{2*}_{2n}(Lk_0) - \frac{1}{\sqrt{6}} D^{2*}_{-2n}(Lk_0) \right] \quad \text{(B19)}$$

and integrating eq B4 over $d\Gamma$ making use of the property[61]

$$\int d\Gamma \, D^p_{ij}(Lk_0) \, D^q_{mn}(Lk_0) = \frac{4\pi}{5} \delta_{pq} \delta_{im} \quad \text{(B20)}$$

we obtain

$$\langle \Delta a_k(t) \rangle = \frac{1}{10} \frac{\beta\alpha E^2 \Delta a}{(N-1)^2} \sum_{nm_1m_2} C(112;00) \times C(112;m_1m_2) \sum_{ij} \langle D^2_{0n}(kk_0) \, D^1_{m_10}(k_0i_0) \, D^1_{m_20}(k_0j_0) \rangle \quad \text{(B21)}$$

Following arguments similar to those preceding eq B14, the average above vanishes unless $n = 0$ and $m_1 + m_2 = 0$. Following some straightforward manipulations, it can be shown

$$\langle \Delta a(\Omega_k) \rangle = \frac{1}{10} \frac{\beta\alpha E^2 \Delta a}{(N-1)^2} \sum_m C(112;00) \, C(112;m,-m) \times \sum_{ij} \langle D^1_{00}(i_0j_0) \, D^1_{0m}(j_0k_0) \, D^1_{0,-m}(j_0k_0) \, D^2_{00}(k_0k) \rangle \quad \text{(B22)}$$

Using $C(112;00) = (2/3)^{1/2}$, $C(112;1\text{-}1) = C(112;\text{-}11) = (1/6)^{1/2}$ along with

$$D^1_{0m} D^1_{0-m} = \frac{1}{3} D^2_{00} - \frac{1}{3} \quad m = \pm 1$$
$$= \frac{2}{3} D^2_{00} + \frac{1}{3} \quad m = 0 \quad \text{(B23)}$$

and summing over k finally yields

$$\langle \Delta a(t) \rangle = \frac{1}{15} \frac{\beta\alpha E^2 \Delta a}{(N-1)^2} \sum_{ijk} \langle D^1_{00}(i_0j_0) \, D^2_{00}(j_0k) \rangle \quad \text{(B24)}$$

for an induced dipole orienting mechanism.

References and Notes

(1) Breslauer, K. J.; Ferrante, R.; Marky, L. A.; Dervan, P.; Youngquist, R. S. *Structure and Expression: Vol. 2, DNA and Its Drug Complexes*; Adenine: New York, 1988; p 273.
(2) Anderson, J. E.; Ptashne, M.; Harrison, S. C. *Nature* **1987**, *326*, 846.
(3) Travers, A.; Klug, A. *Nature* **1987**, *327*, 280.
(4) Kratky, O.; Porod, G. *Recl. Trav. Chim. Pays-Bas* **1949**, *68*, 1106.

(5) Bloomfield, V. A.; Crothers, D. M.; Tinoco, I., Jr. *Physical Chemistry of Nucleic Acids*; Harper & Row: New York, 1974; Chapter 5.
(6) Schurr, J. M.; Schmitz, K. S. *Annu. Rev. Phys. Chem.* **1986**, *37*, 271.
(7) Maret, G.; Weill, G. *Biopolymers* **1983**, *22*, 2727.
(8) Stellwagen, N. C. *Biopolymers* **1981**, *20*, 399.
(9) Elias, J. G.; Eden, D. *Macromolecules* **1981**, *14*, 410.
(10) Hagerman, P. J. *Biopolymers* **1981**, *20*, 1503.
(11) Lewis, R. J.; Pecora, R.; Eden, D. *Macromolecules* **1986**, *19*, 134.
(12) Diekmann, S.; Hillen, W.; Jung, M.; Wells, R. D.; Porschke, D. *Biophys. Chem.* **1982**, *15*, 157.
(13) Diekmann, S.; Hillen, W.; Morgeneyer, B.; Wells, R. D.; Porschke, D. *Biophys. Chem.* **1982**, *15*, 263.
(14) Antosiewicz, J.; Porschke, D. *Biophys. Chem.* **1989**, *33*, 19.
(15) Yamaoka, K.; Fukudome, K. *J. Phys. Chem.* **1990**, *94*, 6896.
(16) Hagermann, P. J.; Zimm, B. H. *Biopolymers* **1981**, *20*, 1481.
(17) Hearst, J. E.; Harris, R. A.; Beals, E. *J. Chem. Phys.* **1967**, *46*, 398.
(18) Soda, K. J. *J. Phys. Soc. Jpn.* **1973**, *35*, 866.
(19) Bixon, M.; Zwanzig, R. *J. Chem. Phys.* **1978**, *68*, 1896.
(20) Moro, K.; Pecora, R. *J. Chem. Phys.* **1978**, *69*, 3254.
(21) Barkley, M. D.; Zimm, B. H. *J. Chem. Phys.* **1979**, *70*, 2991.
(22) Maeda, T.; Fujime, S. *Macromolecules* **1981**, *14*, 809.
(23) Fujime, S.; Maeda, T. *Macromolecules* **1985**, *18*, 191.
(24) Roitman, D. B.; Zimm, B. H. *J. Chem. Phys.* **1984**, *81*, 6333, 6348.
(25) Yoshisaki, T.; Yamakawa, H. *J. Chem. Phys.* **1984**, *81*, 982.
(26) Aragon, S. R.; Pecora, R. *Macromolecules* **1985**, *18*, 1868.
(27) Aragon, S. R. *Macromolecules* **1987**, *20*, 370.
(28) Song, L.; Allison, S. A.; Schurr, J. M. *Biopolymers* **1990**, *29*, 1773.
(29) Lewis, R. J.; Allison, S. A.; Eden, D.; Pecora, R. *J. Chem. Phys.* **1988**, *89*, 2490.
(30) Hagerman, P. J. *Biochemistry* **1985**, *24*, 7033.
(31) Diekmann, S. *FEBS Lett.* **1986**, *195*, 53.
(32) Wu, H.-M.; Crothers, D. M. *Nature* **1986**, *308*, 509.
(33) Ulanovsky, L.; Bodner, M.; Trifonov, E. N.; Choder, M. *Proc. Natl. Acad. Sci. U.S.A.* **1986**, *83*, 862.
(34) Nelson, H. C.; Finch, J. T.; Luisi, B. F.; Klug, A. *Nature* **1987**, *330*, 221.
(35) Allison, S. A.; Austin, R.; Hogan, M. *J. Chem. Phys.* **1989**, *90*, 3843.
(36) Song, L.; Schurr, J. M. *Biopolymers* **1990**, *30*, 229.
(37) Ermak, D. L.; McCammon, J. A. *J. Chem. Phys.* **1978**, *69*, 1352.
(38) Fixman, M. *J. Chem. Phys.* **1978**, *69*, 1527.
(39) Allison, S. A.; McCammon, J. A. *Biopolymers* **1984**, *23*, 363.
(40) Allison, S. A. *Macromolecules* **1986**, *19*, 118.
(41) Fixman, M. *J. Chem. Phys.* **1988**, *89*, 2442.
(42) Iniesta, A.; Garcia de la Torre, J. *J. Chem. Phys.* **1990**, *92*, 2015.
(43) Provencher, S. W. *Comput. Phys. Commun.* **1982**, *27*, 229.
(44) Pecora, R. *Science* **1991**, *251*, 893.
(45) Yamaoka, K.; Matsuda, K. *Macromolecules* **1980**, *13*, 1558.
(46) Ding, D.-W.; Rill, R. L.; van Holde, K. E. *Biopolymers* **1972**, *11*, 2109.
(47) Hogan, M.; Dattagupta, N.; Crothers, D. M. *Proc. Natl. Acad. Sci. U.S.A.* **1978**, *75*, 195.
(48) Yoshioka, K. *J. Chem. Phys.* **1983**, *79*, 3482.
(49) Diekmann, S.; Jung, M.; Teubner, M. *J. Chem. Phys.* **1984**, *80*, 1259.
(50) Yamaoka, K.; Fukudome, K. J. *J. Phys. Chem.* **1988**, *92*, 4994.
(51) Sokerov, S.; Weill, G. *Biophys. Chem.* **1979**, *10*, 161.
(52) Rau, D. C.; Charney, E. *Macromolecules* **1983**, *16*, 1653.
(53) Charney, E. *Quart. Rev. Biophys.* **1988**, *21*, 1.
(54) Oosawa, F. *Polyelectrolytes*; Marcel Dekker: New York, 1971; Chapter 5.
(55) Allison, S. A.; Sorlie, S. S.; Pecora, R. *Macromolecules* **1990**, *23*, 1110.
(56) Garcia de la Torre, J.; Jimenez, A.; Freire, J. J. *Macromolecules* **1982**, *15*, 148.
(57) McQuarrie, D. A. *Statistical Mechanics*; Harper & Row: New York, 1976.
(58) Allison, S. A. *Macromolecules* **1991**, *24*, 530.
(59) Wegener, W. A.; Dowben, R. M.; Koester, V. J. *J. Chem. Phys.* **1979**, *70*, 622.
(60) Schurr, J. M. *Chem. Phys.* **1984**, *84*, 71.
(61) Rose, M. E. *Elementary Theory of Angular Momentum*; John Wiley & Sons: New York, 1957.